RESEARCH ARTICLE
Cytoskeleton, January 2014 71:24–35 (doi: 10.1002/cm.21151)

Causes of Retrograde Flow in Fish Keratocytes

Thomas Fuhs,[1,2]* Michael Goegler,[1] Claudia A. Brunner,[1] Charles W. Wolgemuth,[3] and Josef A. Kaes[1]

[1]Division of Soft Matter Physics Department of Physics, University of Leipzig, 04103 Leipzig, Germany
[2]Paul Flechsig Institute of Brain Research, University of Leipzig, 04109 Leipzig, Germany
[3]Departments of Physics of Molecular and Cellular Biology, University of Arizona, Tucson, Arizona

Received 15 October 2012; Revised 5 August 2013; Accepted 8 October 2013
Monitoring Editor: Pekka Lappalainen

Confronting motile cells with obstacles doubling as force sensors we tested the limits of the driving actin and myosin machinery. We could directly measure the force necessary to stop actin polymerization as well as the force present in the retrograde actin flow. Combined with detailed measurements of the retrograde flow velocity and specific manipulation of actin and myosin we found that actin polymerization and myosin contractility are not enough to explain the cells behavior. We show that ever-present depolymerization forces, a direct entropic consequence of actin filament recycling, are sufficient to fill this gap, even under heavy loads. © 2013 Wiley Periodicals, Inc.

Key Words: cell motility and forces; forces causing retrograde actin flow; polymerization and depolymerization force; actin network and myosin motors; atomic force microscopy

Introduction

Certain aspects of cell movement have been revealed by decades of beautiful and varied studies, and a great deal of our current understanding of cell motility has come from epithelial fish keratocytes. These cells exhibit a highly regular morphology, move fast, and persistently [Lacayo et al., 2007; Keren et al., 2008], and have a thin lamellipodium, all of which make them an ideal subject for investigating the cytoskeletal forces and flows that accompany cell crawling. Different force generating mechanisms have been studied in these cells, including traction forces [Lee et al., 1994; Oliver et al., 1995], whole cell stall measurements [Oliver et al., 1995; Brunner et al., 2006], lamellipodial stall measurements [Prass, 2006; Heinemann et al., 2011; Zimmermann et al., 2012], and hydrodynamic forces due to intracellular fluid flows [Keren et al., 2009]. The role of specific cytoskeletal proteins has been investigated using selective inhibitory drugs [Jurado et al., 2005]. These diverse and detailed findings create an apparently comprehensive understanding of cell movement, yet core pieces of this picture are incomplete. Moreover, former studies have largely been focused on isolated components of cell forces, resulting in fragmented and often apparently contradictory data.

Some force generating mechanisms are based on molecular motors [Sheetz et al., 1992; Finer et al., 1994], swelling gels [Herant et al., 2003] or hydrostatic pressure [Charras et al., 2005]. The most commonly accepted mechanism in cell motility is that lamellipodium protrusion is driven by actin polymerization against the plasma membrane [Theriot and Mitchison, 1991; Carlier et al., 2003; Pollard and Borisy, 2003]. While the cell advances due to actin polymerization, the actin filaments move backward with respect to the substrate, a phenomenon termed retrograde flow (RF) [Vallotton, 2005; Gupton and Waterman-Storer, 2006]. RF can be caused by the work generated through polymerization at the lamellipodium edge that pushes the membrane forward and, consequently, pushes the generated actin network backward [Forscher and Smith, 1988]. In addition, RF links the leading edge to the rest of the cell. In the transition zone between the lamellipodium and cell body, the retrograde flow ceases as actin forms contractile structures with myosin [Svitkina et al., 1997]. The contractile forces generated in these structures can pull the network backwards [Vallotton, 2004]. The actin network has to be recycled to the cell front in a depolymerized state. This ever present depolymerization of the network has received little attention as a source of contractility. This effect has been first proposed for the case of nematode sperm and has only recently been proposed to exist in actin based motility [Wolgemuth et al., 2005; Mseka and Cramer, 2011]. It must exist for any depolymerizing network, since the resulting contraction is an entropic consequence [Sun et al., 2010].

Additional Supporting Information may be found in the online version of this article.
The first three authors contributed equally to this study.
*Address correspondence to: Thomas Fuhs, Division of Soft Matter Physics, Department of Physics, University of Leipzig, Linnéstrasse 5, 04103 Leipzig, Germany. E-mail: TFuhs@physik.uni-leipzig.de
Published online 7 November 2013 in Wiley Online Library (wileyonlinelibrary.com).

Although restraining forces against fibronectin coated beads bound on top of the lamellipodium could be measured by optical trapping [Galbraith and Sheetz, 1999], it has not been possible to measure the forces within the lamellum. These forces are essential for an accurate picture, as they indicate the force balance between lamellipodial edge and cell body, between the wings and central parts of the lamellipodium, and critically reveal how these separate force generation centers physically affect each other.

Our measurement strategy is to measure the forces that stall a cell, or its leading edge, when it pushes against an uncoated, inert polystyrene bead attached to an AFM-cantilever (Fig. 2A). This force is the maximal force the cell can produce. The cantilever measures the height of the bead over the substrate by vertical deflection and the exerted force within the plane of movement by lateral deflection. The bead can be positioned anywhere in front of the leading edge opposing the cell as solid barrier. This method has been shown to work with fish keratocytes [Brunner et al., 2006; Zimmermann et al., 2012] as well as with other cells [Fuhs et al., 2013].

If, instead, the bead sits on the lamellipodium at an arbitrary position, then the bead can be used to measure the forces related to the retrograde actin flow throughout the entire lamellum and lamellipodium. Since the bead is inert, no bio-chemical link is formed between the cell and bead. Therefore, the force on the bead arises due to frictional coupling between the cell and bead, alone. Thus, the forces measured by the cantilever are lower bounds on the forces generated by the cell. Nevertheless, a comparison with literature data [Galbraith and Sheetz, 1999] shows that the frictional coupling is relatively strong, as the measured forces compare well. Since forces only exist in balance with opposing forces, our measurements naturally show a load dependence which culminates in a stall force that arrests motion. The external bead forms an obstacle for membrane flow and cytoskeletal motions, as well as hydrodynamic flows. It measures the integral resulting force that drives the cell's motion at this position. The measurement cannot directly separate force contributions that stem from different sources; however, different cytoskeletal mechanisms can be manipulated through specific cytoskeletal drugs. We can then differentiate between possible origins of forces using these quantitatively measured force values.

While previous measurements addressed only certain cellular forces at specific localizations, we refined our scanning force microscopy (SFM) technique to precisely probe all the dominant forces in a migrating cell, providing a more complete picture of cellular force balance. We complement it with traction force microscopy, which gives an overview of the forces that are transmitted from the cell to the substrate, and lamellipodium feature tracking, to gain access to the retrograde flow velocity. Combining these three measurements, our studies provide a dynamic force map that gives the magnitude and direction of the intracellular forces. Direct measurements of the force within the lamellipodium show that the forward directed forces in the central lamellipodium are generated exclusively at the leading edge, and are independent from the forces moving the cell body. Furthermore, we measure the forces of lamellipodium protrusion, retrograde flow, and cell-body migration as a function of targeted drugs that selectively alter actin polymerization or motor related contractility to reveal the molecular origin of the region-specific forces.

Results

Control Cells

We measured cell speed and retrograde flow throughout the whole lamellipodium of migrating keratocytes using time lapse image series obtained with phase contrast microscopy. The cells moved on average at 10 μm/min (±3.7, STD, n = 52), with a retrograde flow of 4.1 (±1.8) μm/min in the center and 7.7 (±1.9) μm/min in the wings (Figs. 1B and 1C). With our SFM we measured the stall stress of the leading edge in the center of the cell to be 1180 Pa (±370 Pa, n = 33) (Figs. 2 and 3). When the cantilever was sitting on the actin network of the lamellipodium we measured stresses pointing towards the cell body. In the central region, we measured 180 Pa (±70 Pa, n = 28, Figs. 5A–5C) while the stress in the wings was higher at 480 Pa (±270 Pa, n = 28). The force needed to stall the whole cell was 68 nN (±18nN, n = 36, Figs. 4A–4C). Traction force measurements showed the highest forces under the wings, and the forces exerted on the substrate summed up to 100 nN (±20 nN, Fig. 4D).

Myosin Inhibition

We inhibited myosin activity with ML-7 or blebbistatin. The concentrations of these drugs were chosen to have a visible effect on cell speed, while being low enough to ensure some remaining motility (4.9 ± 1.8 μm/min, n = 10, 750 nM ML-7; 3.7 ± 1.5 μm/min, n = 12, 100 μM blebbistatin, Fig. 1B). The cells maintained their general shape, although it was less well defined. For blebbistatin concentrations higher than those used for the measurements, the cells lose their well defined shape (Figs. 1A and 1D).

Both drugs reduced the RF velocity in the whole cell, in the center it went down to 2.5 μm/min (±0.7 μm/min, n = 10, 750 nM ML-7) and 2.4 (±1.1 μm/min, n = 12, 100 μM blebbistatin). In the wings it slowed to 4.2 μm/min (±1.0 μm/min, ML-7) and 2.9 μm/min (± 1.0 μm/min, blebbistatin). For ML-7 treated cells we measured no significant change in the protrusion stress at the leading edge (1310 ± 320 Pa, n = 14), the stress in the central retrograde flow 220 Pa (±120Pa, n = 8, Figs. 5D–5F) or the cell body stall force 55 nN (±13 nN, n = 8). For

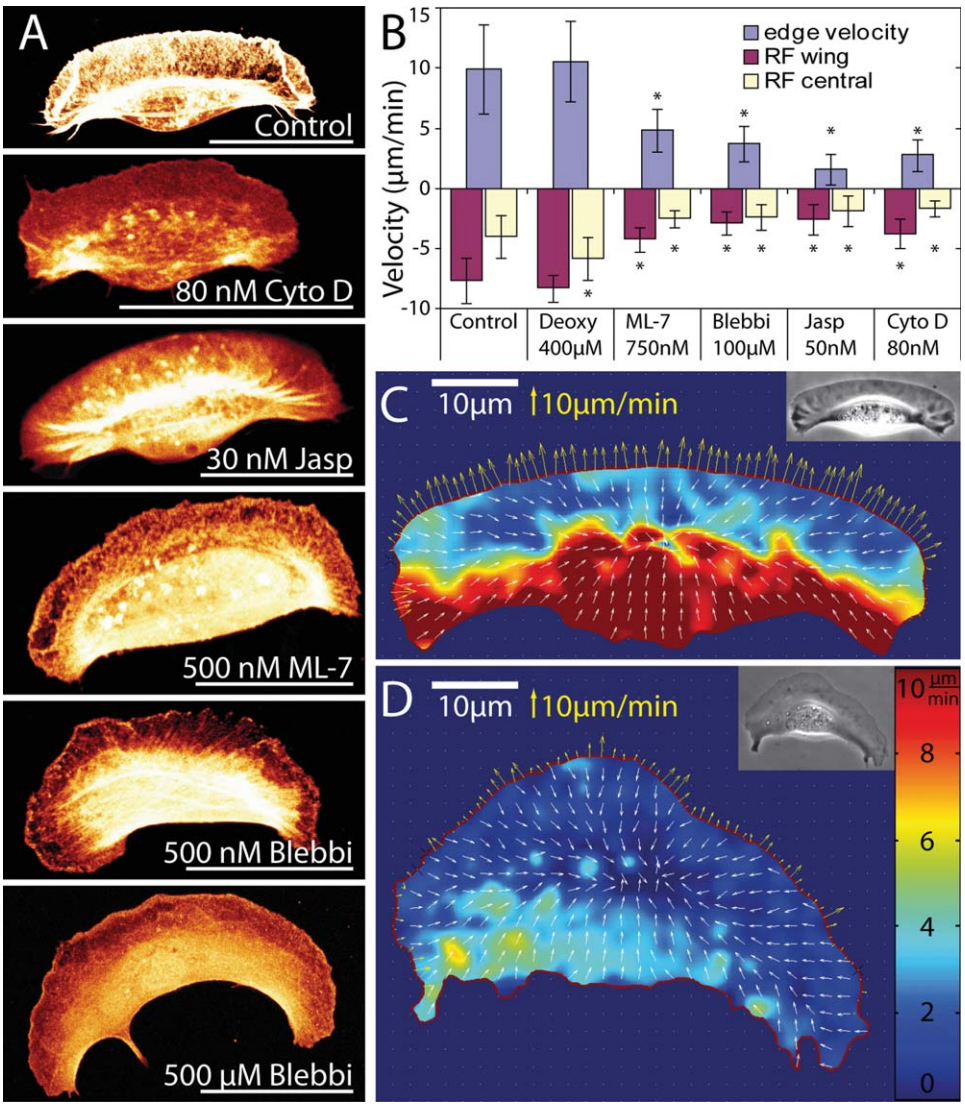

Fig. 1. Changes of different parameters due to molecular alteration. (**A**) Filamentous actin, stained with TRITC-phalloidin, of drug treated keratocytes shown in fluorescence. Cytochalasin D (Cyto D) treated cells show less actin bundles. Jasplakinolide (Jasp) show prominent actin bundles in the back of the cell. The prominent actin rim at the leading edge of the lamellipodium, however, seems to be reduced. High concentrations of blebbistatin (500 µM) led to an almost complete loss of thick actin bundles. Scale bars: 20 µm. (**B**) Protrusion velocity and retrograde flow velocities in the center of the lamellipodium and in the wings are plotted for control and drug treated cells. All drugs decreased protrusion, retrograde flow, and polymerization speeds. (**C**) Edge velocity (yellow arrows) and retrograde flow (white arrows for direction, velocity is color coded, color bar is in panel D) analyzed by feature tracking. The inward flow is strongest in the wings of the keratocyte. (**D**) Edge velocity and retrograde flow of a keratocyte treated with 100 µM blebbistatin. The retrograde flow is slower in the wings compared to untreated keratocytes (compare Fig. 3C).

blebbistatin treated cells the cell body stall force dropped to 25.5 nN (±6.4 nN; Fig. 4C)

Inhibition of Actin Polymerization

We inhibited actin polymerization using cytochalasin D, concentrations of 60–100 nM affected the cells but left them still motile. Cells treated with 80 nM CD moved with speeds of 2.8 µm/min (±1.3 µm/min, $n = 29$), the RF slowed to 1.6 µm/min (±0.7 µm/min) in the center and 3.8 µm/min (±1.2 µm/min) in the wings (Fig. 1B). The protrusion force at the leading edge dropped in a dose-dependent manner to 850 Pa (±170 Pa, 60 nM), 790 Pa (±320 Pa, 80 nM), and 520 Pa (±100 Pa, 100 nM), the same behavior could be seen for the cell body stall forces 48 nN (±10 nN, $n = 5$, 60 nM), 29.4 nN (±8.5 nN, $n = 6$, 80 nM), and 25.3 nN (±3.9 nN, $n = 5$, 100 nM; Figs. 3C and 4C). High doses of 5 µM CD arrest further extension of the leading edge immediately, the cell body catches up and the cell rounds up (Supporting Information Movie S3).

Inhibition of Actin Depolymerization

We used jasplakinolide to inhibit actin depolymerization. Cell speed was reduced to 1.6 µm/min (±1.3 µm/min, $n = 15$, 50 nM), the RF slowed to 1.9 ± 1.2 µm/min in the

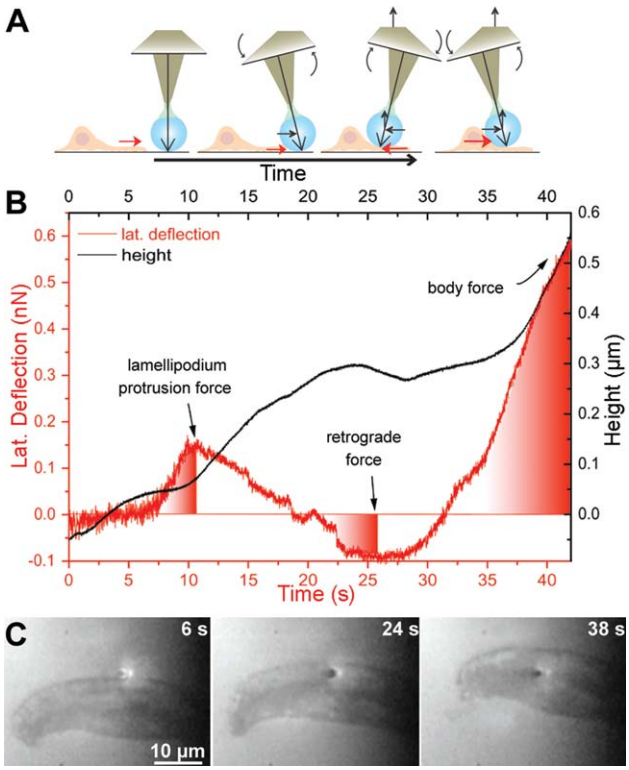

Fig. 2. Experimental principle and force measurement on a fish keratocyte. (**A**) Experimental principle, side view: A cell approaches the bead attached to the cantilever tip and pushes against it, thereby twisting and bending the cantilever (lateral and vertical deflection, the lateral one is in the plane of movement, both are detected via the SFM photodiode). (**B**) SFM-signal of a force measurement. The lateral deflection signal (red) is directly proportional to force and shows three regions of alternating force direction: A forward pushing force at the leading edge, then a force pointing towards the cell body within the lamellum, followed by a forward pushing force in the cell body region. This change in force direction directly suggests that the forces at the leading edge are generated locally and are independent from the force production mechanisms at the cell body. The height signal reflects the typical topography of a fish keratocyte. (**C**) Corresponding image sequence, time given in upper right corner (interference reflection microscopy, IRM). The bead on the cantilever is visible near the center of each image (initially bright spot). [Color figure can be viewed in the online issue, which is available at wileyonlinelibrary.com.]

center and 2.6 ± 1.3 µm/min in the wings (Fig. 1B). The protrusion stress (1190 ± 410 Pa, $n = 14$) and the cell body stall force (56 ± 10 nN, $n = 9$, 30 nM) remained unaffected (Figs. 3C and 4C), and the cells maintained their well defined shape (Fig. 1A). Given higher doses (200 nM) the cell stops moving, although it still generates active lamellipodia (Supporting Information Movie S4).

Softening of the Cell Membrane

We used 400 µM deoxycholate to soften the cell membrane. Cell speed was unaffected (10.6 ± 3.4 µm/min, $n = 10$), and the retrograde flow increased to 5.9 (±1.8) µm/min in the center; however, in the wings the increase in RF to 8.3 (±1.1) µm/min was not significant (Fig. 1B).

Potential Role of Actin Depolymerization in Keratocyte Motility

While some of the results that have been described so far are expected, such as protrusion force decreasing in a dose-dependent manner with cytochalasin D concentration, others were more surprising. For example, it was not expected that ML-7 treatment would not affect the retrograde stress in the actin network, even though cell speed was reduced by over 50%. This finding suggests that myosin contraction of the actin network may not be the principle driving force of the actin retrograde flow in keratocyte motility. Recent experiments and modeling have proposed that depolymerization of the cytoskeleton may play a substantial role in force generation in motile cells [Wolgemuth et al., 2005; Sun et al., 2010; Mseka and Cramer, 2011; Shimabukuro et al., 2011].

In order to test whether actin disassembly could be producing a significant fraction of the force in migrating keratocytes, we developed a model that accounts for disassembly driven forces, based on the previous modeling that has been done for nematode sperm cells [Zajac et al., 2008]. A solution of polymer filaments that can interact or be cross-linked to one another experiences two competing forces. Entropy (i.e., thermal fluctuations) try to spread the filaments apart, while attractive interactions and cross-links hold the network together. These two competing forces can balance one another at a specific concentration of polymer. Any deviations from this preferred concentration will then lead to stress in the network [Sun et al., 2010]. Since depolymerization reduces the concentration, the remaining polymer will contract to attempt to fill in for the lost material. This contraction is driven by the enthalpy of the interaction between the actin filaments, whether it be an actin–actin interaction or an interaction due to crosslinks. Our model treats the actin cytoskeleton as a viscous fluid that compresses due to depolymerization and experiences resistive drag from the substrate (a complete description of the mathematics is given in the "Experimental Procedures" section). To begin, we used a one-dimensional version of our depolymerization force model to calculate the stresses along the center of the cell parallel with the direction of motion originating from the inherently present depolymerization of the actin network. The model clearly predicts our SFM data on the forces that occur in the central lamellipodium, for both control cells and keratocytes treated with ML-7 (Fig. 5). The depolymerization rates (7.0 ± 2.6 and 3.5 ± 1.4 min^{-1}) are similar to rates reported for other cells [Theriot and Mitchison, 1991; Pollard et al., 2000; Watanabe, 2002] and the model captures the behavior after the flow reverses direction in front of the cell body.

It is interesting that the depolymerization model, which does not account for myosin activity, can accurately predict the flows and stresses in these cells. However, since our

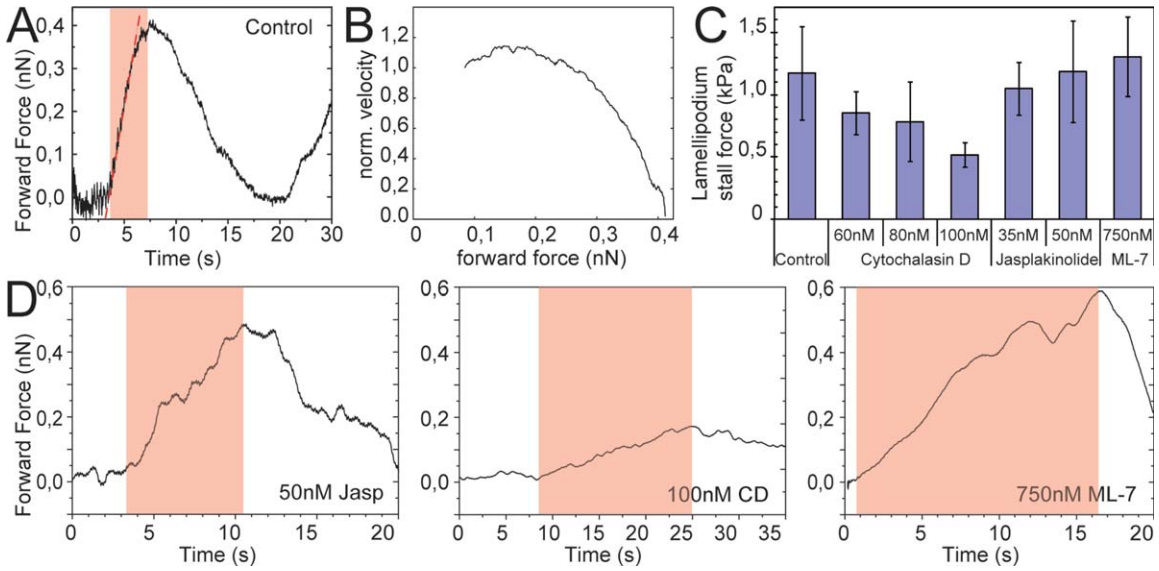

Fig. 3. Lamellipodium protrusion force. (**A**) Lateral force build up during lamellipodium stall force experiment (red shadowed data are the bases for the force–velocity curve). (**B**). Normalized time derivative of lateral deflection plotted versus forward force results in a force–velocity curve for the lamellipodium which shows a concave behavior. (**C**) Lamellipodium stall force experiments reveal a significant reduction in stall pressure for cells treated with cytochalasin D. Jasplakinolide and ML-7 treatments show no effect. (**D**) Lamellipodium stall force data for cells treated with different cytoskeletal drugs: ML-7 and jasplakinolide clearly slow down the force build-up, but do not decrease maximum forces, whereas cytochalasin D also decreases maximum lamellipodial stall forces. [Color figure can be viewed in the online issue, which is available at wileyonlinelibrary.com.]

model was one-dimensional, we could only calculate flows along the center of the cell. Therefore, we generalized our model to 2D in order to more fully investigate what flows were predicted. We simulated this 2D model using geometries defined by our experimental images. We assumed stress free boundaries and that the front half of the cell polymerized new actin at the preferred concentration. We then determined what value of the depolymerization rate would

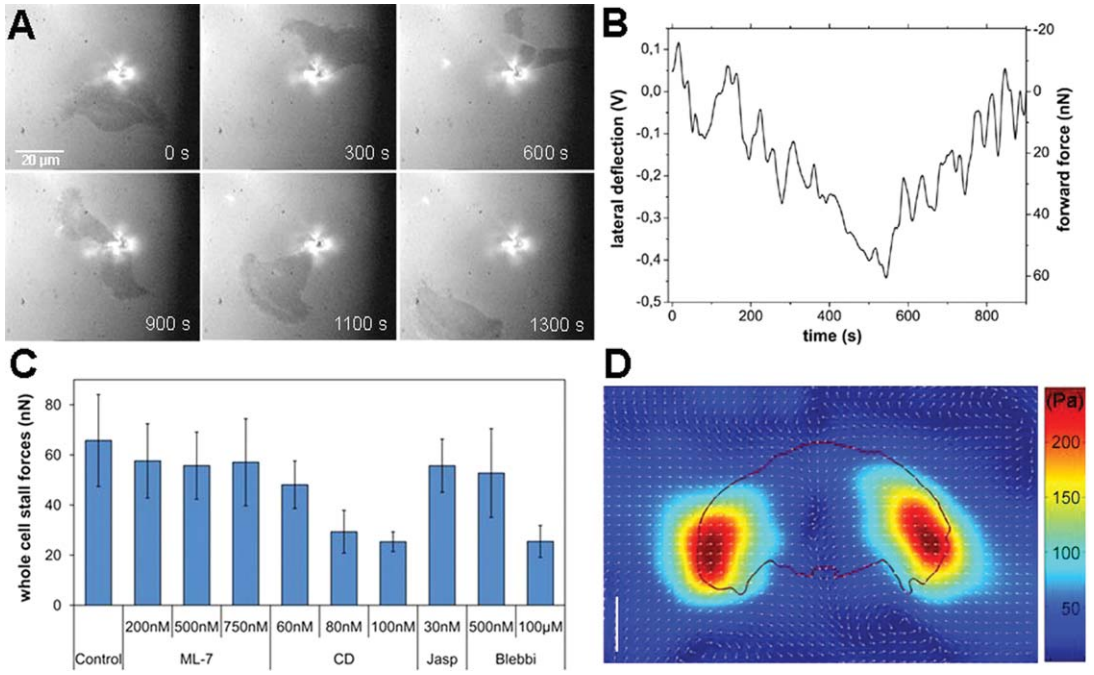

Fig. 4. Cell body stall force measurements and traction force distribution. (**A**) Time series of a stalled keratocyte observed in IRM (Supporting Information Movie S2). (**B**) Corresponding force signal. The maximum force is reached when the lateral flanks eventually become the front of the cell as shown in A. (**C**) Cell body stall force dependence on drug type and concentration. Only cytochalasin D (CD 80 nM, 100 nM) or high concentrations of blebbistatin led to a significant reduction in body force. (**D**) Traction force measurements reveal the strongest forces in the wings of a keratocyte. Arrows indicate the direction of the force. Outline of the cell is given in red. Scale bar: 10 µm.

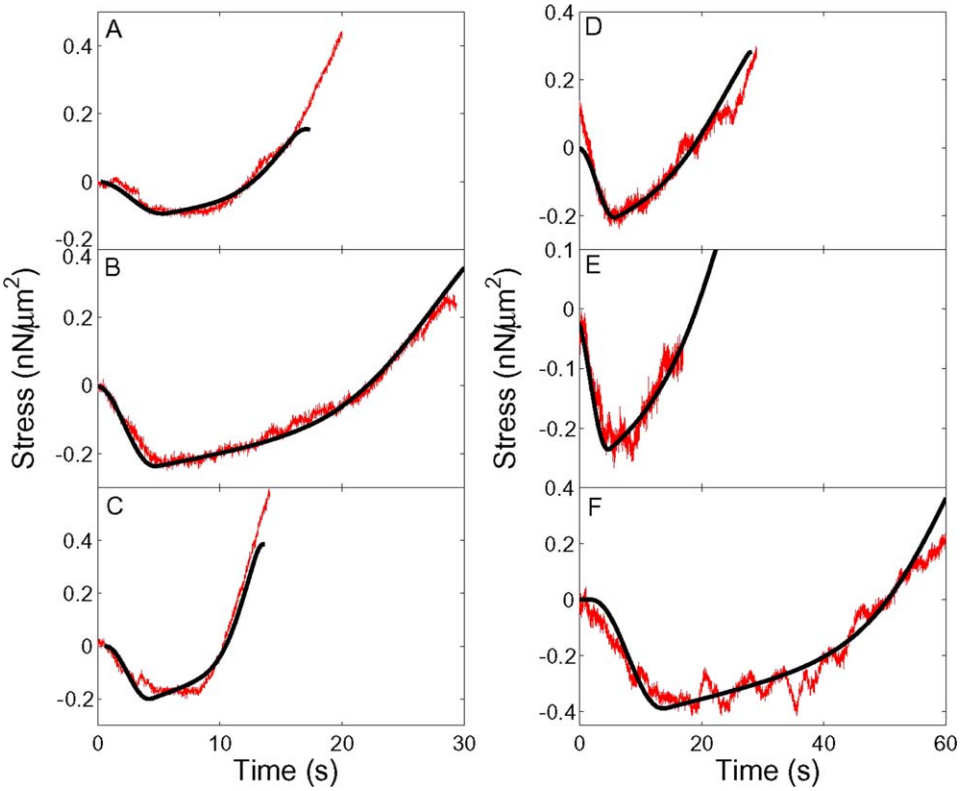

Fig. 5. Representative SFM data and fits from the depolymerization-induced contraction model. Panels (**A–C**) show data from untreated keratocytes, and panels (**D–F**) are for keratocytes treated with 750 nM ML-7. The force curve in panel A is the negative section of the force curve of Fig. 2B. For the untreated cells, the fits to the data give estimates for the ratio of the drag coefficient to the stress coefficient, $\tilde{\zeta} = 0.0022 \pm 0.0012$ min/μm, and the depolymerization rate, $\gamma = 7.0 \pm 2.6$ min^{-1}. We find values of $\tilde{\zeta} = 0.0017 \pm 0.0012$ min/μm and $\gamma = 3.5 \pm 1.4$ min^{-1} with the ML-7 treated cells. [Color figure can be viewed in the online issue, which is available at wileyonlinelibrary.com.]

produce the correct velocity at the rear of the cell. We simulated control cells and cells treated with 100 μM blebbistatin, 50 nM jasplakinolide or 80 nM cytochalasin D. Our model predicted that the depolymerization rates for these cases were 1.0 min^{-1} (control), 0.24 min^{-1} (blebbistatin), 0.48 min^{-1} (jasplakinolide), and 0.12 min^{-1} (cytochalasin D). In agreement with these predictions, previous work has shown that a 50 nM solution of jasplakinolide should decrease the actin depolymerization rate by approximately 50%, which is exactly what is predicted by our model [Bubb, 2000]. In Fig. 6 panels A and E, the major difference between the simulation and control cells is that the model does not predict the correct flow in the wings of the cell. The experiment shows larger flows perpendicular to the direction of motion than the model does, as is expected if myosin is contracting bundled actin at the rear of the cell. The model does a much better job predicting the 2D flow of actin in blebbistatin-treated cells and even in jasplakinolide and cytochalasin D treated cells.

Discussion

We see three different contributors to keratocyte motility (Fig. 7). First myosin as a molecular motor is one key factor. Inhibition of myosin drastically reduces the cell speed. The RF velocity in the wings and the central region of the lamellipodium decreases as well. Given low doses of myosin inhibitors the cell can maintain its shape. For higher concentrations cells are still motile but lose their well defined shape and fragments of the lamellipodium can break from the cell and move on independently. Combined with the flow field simulations that are unable to reproduce the fast actin flow in the wings we conclude that myosin activity is important in the back of the cell where it keeps the cell in shape and generates the traction forces. This is supported by the work of Yam et al. [2007] who showed that myosin activity is important to initiate cell polarity and thereby motility. It was also observed for other cell types [Even-Ram et al., 2007]. But even at high concentrations of myosin inhibitors the RF does not stop completely. It must be kept up by some other force, this brings actin into focus.

We measured a forward directed stress of 1.2 kPa at the leading edge, with 1.3 kPa it remains unchanged upon myosin inhibition. Giardini et al. [2003], Marcy et al. [2004], and Parekh et al. [2005] measured the stress generated by actin polymerizing against beads or AFM cantilevers in vitro, their values deviate only slightly from the stress we measured. This shows that the stress we measured

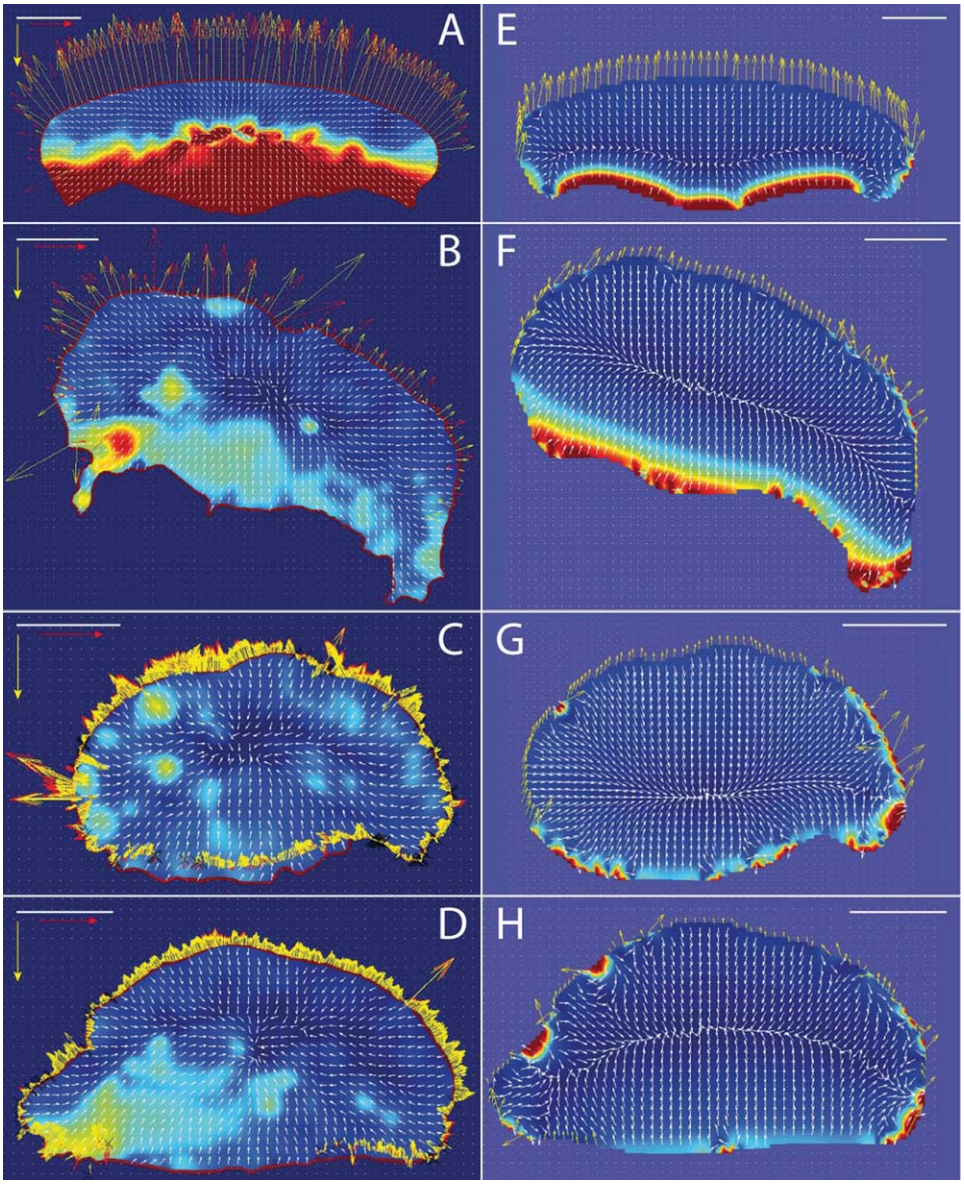

Fig. 6. Comparison of the 2D model to measured actin flows in migrating fish keratocytes. The left panels show the measured cytoskeletal flows (white arrows) and boundary (yellow) and computed polymerization (red) velocities for control (**A**), 100 μM blebbistatin (**B**), 50 nM jasplakinolide (**C**), and 80 nM cytochalasin (**D**) treated cells. Panels (**E–H**) show the corresponding simulation results. The white arrows show the direction of the flow and the color map shows the magnitude, which goes from 0 (dark blue) to 10 μm/min (red), the red and yellow scaling arrows with indicate 10 μm/min, the scale bar is 10 μm.

at the leading edge can be generated by actin polymerization alone. This is the second force generating mechanism. It drives the leading edge forward. At the same time we recorded retrograde stress of 180 Pa in the lamellipodium. Again it is not lowered (220 Pa) by myosin inhibition. Since the height of the lamellipodium is fairly constant, the stress generated at the leading edge is more than enough to push the actin network backwards with the measured retrograde stress. This mechanism can explain why the stresses are not influenced by myosin inhibition. Yet this mechanism cannot explain how the cell body can follow the advancing actin network. The stress generated at the leading edge is pointing in the wrong direction at the cell body. The cell body needs a contractile element connecting it to the advancing actin network to follow. Here we have shown that depolymerization-induced contractile forces can account for this needed element (Fig. 5). Our model captures the behavior of the retrograde flow and also correctly predicts the reversal in flow in front of the cell body. In addition, the model predicts that the depolymerization rate of actin is lower in cells treated with ML-7 and blebbistatin, which is consistent with the recent finding that myosin activity increases depolymerization of actin in keratocytes [Wilson et al., 2010].

The tension in the plasma membrane was measured to be 30 pN/μm in NIH 3T3 cells [Raucher and Sheetz,

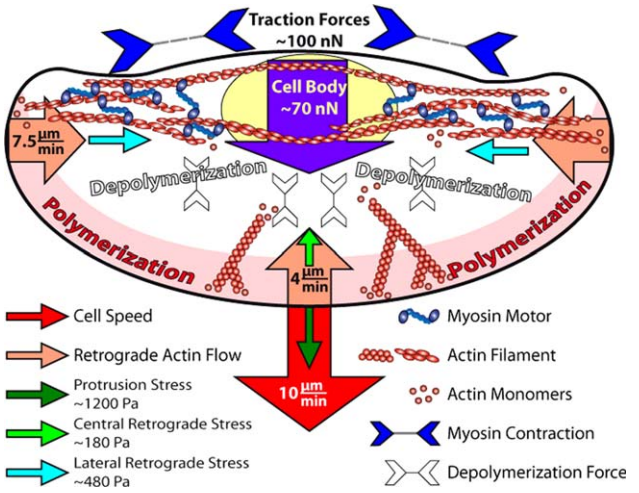

Fig. 7. Illustration of the measured parameters for a migrating fish keratocyte. The force measurements and the characterization of the internal actin dynamics result in an almost complete physical picture for this cell type. Cell body force (violet), lamellipodium velocity and stall stress (red), retrograde actin flow, and stress in the central lamellum (light blue) and inward actin flow, and stress in the lateral lamellum (dark blue) are illustrated. [Color figure can be viewed in the online issue, which is available at wileyonlinelibrary.com.]

2000], but data for keratocytes, is, to our knowledge, not available. At the leading edge this is no match for actin polymerization that produces 300 pN/μm even if the lamellipodium is just 250 nm high. Still 30 pN/μm is close enough to the measured retrograde stress of 200 pN/μm^2 if the lamellipodium is well below 1 μm in height. If the retrograde flow is actin pushing itself away from the membrane, then softer membranes should decrease retrograde flow, but we could measure a slight but significant increase. If the cell body is dragged along in a bag of plasma membrane, or if the plasma membrane crushes the actin filaments at the rear end [Mogilner and Rubinstein, 2010], a softer bag will carry less force slowing the cell down, but cell speed was unaffected in our measurements.

Our measurements with actin targeting drugs support the hypothesis that actin depolymerization is the third force generating mechanism; the one driving the RF. Stabilizing actin filaments with jasplakinolide has no effect on the maximal stall stress at the leading edge and the cell body stall force. At the leading edge the protrusion force is generated by polymerizing filaments at the front of the actin network. The cell body stall force is generated by stress fibers spanning to the back of the cell. The ability to polymerize a well cross-linked, long-fibered actin network with working myosin motors are necessary and none of these are affected by this drug. Still the RF velocity goes down, as can be expected for decreased depolymerization forces. For cytochalasin D the stall stress at the leading edge goes down with increasing concentration, as less filament ends are available for polymerization. The shorter filaments in the actin network generate lower depolymerization forces, leading to a slowed down RF. The cell body stall force is lower, as shorter actin filaments allow fewer myosins to attach per filament, leading to less efficient stress fibers.

The pressure associated with hydrodynamic flow was measured to be in the range of 10 s of Pa [Keren et al., 2009] throughout the cell. This is an order of magnitude below the lowest stress we measured.

Of course we cannot exclude other mechanisms to be active with absolute certainty. We tried to find a minimal model and concentrated on actin and myosin. We ignored intermediate filaments and microtubules as they have, to the best of our knowledge, no influence on keratocyte motility.

In summary our data shows that the keratocyte's motility and retrograde actin flow is influenced by all kinds of drugs affecting the actin–myosin machinery. Working in a low concentration regime we see that the three mechanisms cannot be decoupled completely as they all influence the actin cytoskeleton in their own way. But we could detangle them far enough to show the presence and influence of each of them. We introduced the inherently present depolymerization forces and showed that they are sufficient to drive the retrograde flow observed. The inclusion of the depolymerization force allows explaining the effects of the different drugs we used without introducing any new biochemical feedback loops.

Experimental Procedures

Cell Culture

Primary goldfish epithelial keratocytes were cultured in Dulbecco's modified Eagle's medium (DMEM, E15-810, PAA) supplemented with 20% fetal calf serum (A15-043, PAA), 10 mM HEPES (H4034, Sigma), and 100 U/mL penicillin–streptomycin (P0781, Sigma) in a custom built experimental dish, which consists of a Petri dish with a 3 cm hole in the bottom and a 4 cm round glass cover slip (631-0177, VWR International) glued to it. The cells were cultured at room temperature and 5% CO_2.

Drugs

The application of specific antagonistic drugs allows us to distinguish local contributions of different potential cytoskeleton forcing mechanisms to cell migration.

We deliberately used low drug concentrations for two reasons, first we wanted to measure the cells in a steady, yet altered, state to ensure reproducibility. Drugs were therefore added at least 8h prior to measurement. Second the force measurements require the cells to move.

The effectiveness and selectiveness to their specific cytoskeletal targets—actin (de-) polymerization, myosin activity and membrane tension—was tested with fluorescent staining of the actin cytoskeleton. Cells were clearly affected as evinced by the morphological changes of the cells (Fig. 3A).

Table I. Data Overview

	Edge velocity (μm/min)	Central RF (μm/min)	Wing RF (μm/min)	Leading edge stall stress (Pa)	Central retrograde stress (Pa)	Wing retrograde stress (Pa)	Whole cell stall force (nN)
Control	10.0 (3.7)	4.1 (1.8)	7.7 (1.9)	1175 (373)	180 (70)	480 (270)	66 (18)
CD 60 nM	–	–	–	854 (170)	–	–	48 (9)*
80 nM	2.8 (1.3)*	1.6 (0.7)*	3.8 (1.2)*	785 (319)*	–	–	29 (8)*
100 nM	–	–	–	518 (96)*	–	–	25(4)*
Jasp 30 nM	–	–	–	1050 (213)	–	–	56 (10)
50 nM	1.6 (1.3)*	1.9 (1.2)*	2.6 (1.3)*	1188 (407)	–	–	–
ML-7 200 nM	–	–	–	–	–	–	58 (15)
500 nM	–	–	–	–	–	–	56 (13)
750 nM	4.9 (1.8)*	2.5 (0.7)*	4.2 (1.0)*	1305 (317)	220 (120)	–	57 (17)
Blebbi 500 nM	–	–	–	–	–	–	53 (18)
100 μM	3.7 (1.5)*	2.4 (1.1)*	2.9 (1.0)*	–	–	–	25 (6)*
Deoxy 400 μM	10.6 (3.4)	5.9 (1.8)*	8.3 (1.1)	–	–	–	–

Overview of the measured velocities, stresses, and forces. Significance was tested with Student's *t*-test, significant differences ($P < 0.05$) are marked with *.

Cytochalasin D (C2618, Sigma) inhibits polymerization by capping the actin filaments barbed ends, jasplakinolide (J4580, Sigma) elongates actin filaments by reducing polymerization and depolymerization [Cramer, 1999]. Myosin motor proteins are inhibited by ML-7 (I2764, Sigma) which blocks myosin light chain kinase (MLCK), and blebbistatin (B0560, Sigma), which binds to myosin II [Shu, 2005]. Deoxycholate (D6750, Sigma) softens the cell membrane, the used concentration of 400 μM caused a 50–65% decrease in membrane tension in NIH3T3 and HeLa cells [Raucher, 1999; Raucher and Sheetz, 2000].

Protrusion Force at the Leading Edge

All SFM measurements were done with a Nano Wizard I from JPK (Berlin, Germany) mounted on an inverted microscope (DM IRB, Leica Microsystems, Wetzlar, Germany). The SFM cantilever (Pointprobe, NanoWorld, Neuchâtel, Switzerland) was modified with an attached polystyrene bead (3 or 6 μm) [Mahaffy et al., 2000], we assume the bead to be inert as we did not observe membrane tethers or cells attached to the bead. It was positioned with a preset force on the substrate in front of a migrating fish keratocyte (Fig. 1A, Supporting Information Movie S1). When the cell makes contact to the bead it will push the bead both vertically and laterally. The lateral movement of the bead led to a torsion of the cantilever. As vertical and torsional spring constant of the cantilever are connected material constants protrusion forces can be calculated from the lateral deflection of the cantilever. Maximum protrusion forces were measured when we locally stalled the leading edge motion with the SFM-probe, visible by a clear indentation in the lamellipodium in interference reflection microscopy (IRM) images (Figs. 2A and 2B; preset vertical force ~10 nN). The force build-up (Fig. 2B) in the stall force measurements allowed us to determine the force–velocity curves (Fig. 2C), which have concave shapes. Forward directed stress was calculated assuming an average lamellipodial height of 250 μm to determine the area of the bead that is in contact with the cell.

Retrograde Force in the Lamellum

After a stalling the leading edge the keratocyte can slide under the bead (Figs. 1B and 1C, Supporting Information Movie S1). Once the bead is on top of the cell, it indents the cell while the cell moves underneath. Since the attached polystyrene bead does not adhere to the cell membrane nor a bio-chemical adhesions formed, the net lateral force that the bead experiences reflects the motion of the actin cytoskeleton as well as the cytosolic flows under the bead. Considering that the lamellipodium is a very thin structure (<1 μm) the range in which the bead indentation depth could be varied is too small to observe any significant depth-dependent behavior. The average indentation for a given downward force was extracted from the force-indentation-curves. The effective cross-section for the retrograde stress (0.7 μm^2 for control cells and 1.5 μm^2 for ML-7) was calculated for each drug concentration using the corresponding indentation. As bead might not couple perfectly to the actin network, this measurement can underestimate the true stresses, and should be seen as a lower bound.

Cell Body Force

The cell body force was measured in the same way as the protrusion and retrograde force, albeit stiffer cantilevers

and higher downward forces were used. Only beads of 6 μm diameter were used. The whole cell stall force is predominantly determined by the forces which pull the cell body in a migrating cell, referred to as cell body forces. A measurement was considered successful when the cell could not pass the bead and either stopped translocation or moved in the opposite direction (Fig. 4A).

Traction Force, Velocity, and Cell Elasticity Measurements

Traction forces measurements were performed as described in Fuhs et al. (2013), using polyacrylamide hydrogels with a Young's modulus of 6 kPa.

Edge protrusion velocity and retrograde flow data were obtained by phase contrast feature tracking [Betz et al., 2006; Knorr et al., 2011] of the internal actin transport/flow [Figs. 3C and 3D).

Cell elasticity was determined using a SFM as described in [Mahaffy et al., 2004] using a JPK Nano Wizard I.

Depolymerization Forces

The retrograde force further back in the lamellipodium can be generated by the inherently present depolymerization of the actin cytoskeleton through a process similar to that in crawling nematode sperm cells [Miao, 2003; Wolgemuth et al., 2005; Zajac et al., 2008]. Our calculation of depolymerization forces are based on four assumptions. First, the viscoelastic actin cytoskeleton can be treated as a viscous fluid on time scales relevant for cell migration Rubinstein et al., 2009]. Second, we assume that dynamic crosslinking produces an attractive polymer–polymer interaction between nearby actin filaments. Third, we treat the interaction between the polymer and the substrate using a viscous drag force; i.e., motion of the polymer with respect to the substrate is resisted by a force that is proportional to the polymer velocity. Finally, in the cytoskeletal region that is sandwiched between the SFM probe and the substrate, the fluid velocity is negligible.

In a solution of polymer filaments that are attracted to one another or can crosslink, the total free energy of the system is determined by the sum of the enthalpy (which is predominantly due to the chemical energy stored in the crosslinks, etc.) and entropy (which is a measure of the randomness produced by thermal fluctuations). When the free energy is written in terms of the fraction of filaments per volume (ϕ) the magnitude of the stress is approximately equal to

$$\sigma \approx \frac{k_B T \phi_0^2}{3V_s}(\phi_0 - \phi)\delta_{ij} \tag{1}$$

where k_BT is thermal energy, ϕ_0 is the preferred volume fraction of the polymer solution, V_s is the volume of a monomer, and δ_{ij} is the Kronecker delta function. Deviations from the preferred volume fraction produce a net pressure in the F-actin that acts to drive the F-actin back to this preferred volume fraction. When $\phi \sim \phi_0$, the effective stiffness of the F-actin network (or the hydrostatic compressibility) is $\sigma_0 = k_B T \phi_0^2 / V_s$, which is approximately equal to 103 N/m^2.

Forces that are derived from this stress are balanced by viscous sliding of the actin with respect to itself, movement of the actin through the cytosolic fluid, and by drag between the actin and the substrate. We assume that the substrate drag force dominates and consider a one dimensional problem where the cell crawls in the x direction and the lamellipod has length L. We balance the force due to polymer deformation (the gradient of the stress) by a viscous drag force due to sliding of the actin against the substrate, $\varsigma v = -\sigma_0 \partial\phi/\partial x$, where ζ is a drag coefficient. There is also a frictional drag coefficient for sliding of the actin against the bead (η), but we assume that this is small compared to ζ. The actin depolymerizes via a first order reaction with rate γ.

Therefore, the time evolution of the volume fraction is given by

$$\frac{\partial \phi}{\partial t} = -\frac{\partial}{\partial x}(\phi \upsilon) - \gamma\phi. \tag{2}$$

If the cell is crawling at a constant velocity V_0, then the steady state solution in the frame of the cell is given by $\partial\phi/\partial t = -V_0 \partial\phi/\partial x$. The resulting equation is

$$\frac{\partial}{\partial x}\left(\phi \frac{\partial \phi}{\partial x}\right) + \tilde{\zeta}\left(\frac{\partial \phi}{\partial x} - \gamma\phi\right) = 0 \tag{3}$$

where $\tilde{\zeta} = \varsigma/\sigma_0$. We assume a stress free boundary condition at the front and rear of the cell, $\phi(0) = \phi(L) = \phi_0$, and we assume that $\phi_0 = 0.05$. If the force from depolymerization is to pull the rear of the cell forward, then the velocity at the rear of the lamellipod is equal to the crawling velocity. Therefore, $\partial\phi/\partial x|_0 = -\tilde{\zeta}\, V_0$. This condition sets the value of γ. We solve Eq. 3 using MATLAB's built in function bvp4c. The force per length exerted on the SFM tip due to the actin flow is then computed as $-\eta \partial\phi/\partial x$ $Z\zeta$. From internal reflection microscopy images that are taken simultaneously with the SFM data, it is possible to measure the crawling velocity and the length of time between the collision of the bead with the leading edge and the subsequent impact with the cell body. These two values determine the effective length of the lamellipodium. With these parameters set, there are two free parameters for fitting the data, η and $\tilde{\zeta}$.

For the 2D model, we take into account the viscosity of the cytoskeleton, μ. Therefore, the equations that we solve are

$$\begin{aligned} -\mathbf{V}_0 \cdot \nabla\phi &= \phi_0(\nabla \cdot \mathbf{v}) - \gamma\phi \\ \zeta \mathbf{v} &= \frac{\mu}{2}\nabla \cdot \left(\nabla \mathbf{v} + (\nabla \mathbf{v})^T\right) - \sigma_0 \nabla\phi \end{aligned} \tag{4}$$

where $\mathbf{V}_0$ is the steady crawling velocity and the superscript T denotes the transpose. For all simulations, the velocity $\mathbf{V}_0$

was given by the experimentally determined value of the crawling velocity, and we used $\mu/\varsigma = 1$, $\sigma_0/\varsigma = 5$, and $\phi_0 = 0.05$.

Acknowledgments

This study was supported by the Deutsche Forschungsgemeinschaft with a grant to the Research Training School "InterNeuro" (GRK 1097) and the BMBF-project "Exprimage."

References

Betz T, Lim D, Käs JA. 2006. Neuronal growth: a bistable stochastic process. Phys Rev Lett 96:098103.

Brunner CA, Ehrlicher A, Kohlstrunk B, Knebel D, Käs JA, Goegler M. 2006. Cell migration through small gaps. Eur Biophys J 35:713–719.

Bubb MR. 2000. Effects of jasplakinolide on the kinetics of actin polymerization. An explanation for certain in vivo observations. J Biol Chem 275:5163–5170.

Carlier M-F, Wiesner S, Le Clainche C, Pantaloni D. 2003. Actin-based motility as a self-organized system: mechanism and reconstitution in vitro. C R Biol 326:161–170.

Charras GT, Yarrow JC, Horton MA, Mahadevan L, Mitchison TJ. 2005. Non-equilibration of hydrostatic pressure in blebbing cells. Nature 435:365–369.

Cramer LP. 1999. Role of actin-filament disassembly in lamellipodium protrusion in motile cells revealed using the drug jasplakinolide. Curr Biol 9:1095–1105.

Even-Ram S, Doyle AD, Conti MA, Matsumoto K, Adelstein RS, Yamada KM. 2007. Myosin IIA regulates cell motility and actomyosin–microtubule crosstalk. Nat Cell Biol 9:299–309.

Finer JT, Simmons RM, Spudich JA. 1994. Single myosin molecule mechanics: piconewton forces and nanometre steps. Nature 368: 113–119.

Flory PJ. 1953. Principles of Polymer Chemistry. Ithaca: Cornell University Press.

Flory PJ. 1956. Phase equilibria in solutions of rod-like particles. Proc R Soc A: Math Phys Eng Sci 234:73–89.

Forscher P, Smith SJ. 1988. Actions of cytochalasins on the organization of actin filaments and microtubules in a neuronal growth cone. J Cell Biol107:1505–1516.

Fuhs T, Reuter L, Vonderhaid I, Claudepierre T, Käs JA. 2013. Inherently slow and weak forward forces of neuronal growth cones measured by a drift-stabilized atomic force microscope. Cytoskeleton 70:44–53.

Galbraith CG, Sheetz MP. 1999. Keratocytes pull with similar forces on their dorsal and ventral surfaces. J Cell Biol 147:1313–1324.

Giardini PA, Fletcher DA, Theriot JA. 2003. Compression forces generated by actin comet tails on lipid vesicles. Proc Natl Acad Sci USA 100:6493–6498.

Gupton SL, Waterman-Storer CM. 2006. Spatiotemporal feedback between actomyosin and focal-adhesion systems optimizes rapid cell migration. Cell 125:1361–1374.

Heinemann F, Doschke H, Radmacher M. 2011. Keratocyte lamellipodial protrusion is characterized by a concave force-velocity relation. Biophys J 100:1420–1427.

Herant M, Marganski WA, Dembo M. 2003. The mechanics of neutrophils: synthetic modeling of three experiments. Biophys J 84: 3389–3413.

Jurado C, Haserick JR, Lee J. 2005. Slipping or gripping? fluorescent speckle microscopy in fish keratocytes reveals two different mechanisms for generating a retrograde flow of actin. Mol Biol Cell 16:507–518.

Keren K, Yam PT, Kinkhabwala A, Mogilner A, Theriot JA. 2009. Intracellular fluid flow in rapidly moving cells. Nat Cell Biol 11: 1219–1224.

Keren K, Pincus Z, Allen GM, Barnhart EL, Marriott G, Mogilner A, Theriot JA. 2008. Mechanism of shape determination in motile cells. Nature 453:475–480.

Knorr M, Koch D, Fuhs T, Behn U, Käs JA. 2011. Stochastic actin dynamics in lamellipodia reveal parameter space for cell type classification. Soft Matter 7:3192.

Lacayo CI, Pincus Z, VanDuijn MM, Wilson CA, Fletcher DA, Gertler FB, Mogilner A, Theriot JA. 2007. Emergence of large-scale cell morphology and movement from local actin filament growth dynamics. PLoS Biol 5:e233.

Lee J, Leonard M, Oliver T, Ishihara A, Jacobson K. 1994. Traction forces generated by locomoting keratocytes. J Cell Biol 127:1957–1964.

Mahaffy RE, Park S, Gerde E, Käs J, Shih CK. 2004. Quantitative analysis of the viscoelastic properties of thin regions of fibroblasts using atomic force microscopy. Biophys J 86:1777–1793.

Mahaffy RE, Shih CK, MacKintosh FC, Käs J. 2000. Scanning probe-based frequency-dependent microrheology of polymer gels and biological cells. Phys Rev Lett 85:880.

Marcy Y, Prost J, Carlier M-F, Sykes C. 2004. Forces generated during actin-based propulsion: a direct measurement by micromanipulation. Proc Natl Acad Sci USA 101:5992–5997.

Miao L. 2003. Retraction in amoeboid cell motility powered by cytoskeletal dynamics. Science 302:1405–1407.

Mogilner A, Rubinstein B. 2010. Actin disassembly "clock" and membrane tension determine cell shape and turning: a mathematical model. J Phys: Condens Matter 22:194118.

Mseka T, Cramer LP. 2011. Actin depolymerization-based force retracts the cell rear in polarizing and migrating cells. Curr Biol 21: 2085–2091.

Oliver T, Jacobson K, Dembo M. 1995. Traction forces in locomoting cells. Cell Motil Cytoskeleton 31:225–240.

Parekh SH, Chaudhuri O, Theriot JA, Fletcher DA. 2005. Loading history determines the velocity of actin-network growth. Nat Cell Biol 7:1219–1223.

Pollard TD, Blanchoin L, Mullins RD. 2000. Molecular mechanisms controlling actin filament dynamics in nonmuscle cells. Annu Rev Biophys Biomol Struct 29:545–576.

Pollard TD, Borisy GG. 2003. Cellular motility driven by assembly and disassembly of actin filaments. Cell 112:453–465.

Prass M. 2006. Direct measurement of the lamellipodial protrusive force in a migrating cell. J Cell Biol 174:767–772.

Raucher D. 1999. Membrane expansion increases endocytosis rate during mitosis. J Cell Biol 144:497–506.

Raucher D, Sheetz MP. 2000. Cell spreading and lamellipodial extension rate is regulated by membrane tension. J Cell Biol 148: 127–136.

Rubinstein B, Fournier MF, Jacobson K, Verkhovsky AB, Mogilner A. 2009. Actin-myosin viscoelastic flow in the keratocyte lamellipod. Biophys J 97:1853–1863.

Sheetz MP, Wayne DB, Pearlman AL. 1992. Extension of filopodia by motor-dependent actin assembly. Cell Motil Cytoskeleton 22: 160–169.

Shu S. 2005. Blebbistatin and blebbistatin-inactivated myosin II inhibit myosin II-independent processes in Dictyostelium. Proc Natl Acad Sci USA 102:1472–1477.

Sun SX, Walcott S, Wolgemuth CW. 2010. Cytoskeletal cross-linking and bundling in motor-independent contraction. Curr Biol 20:R649–R654.

Svitkina TM, Verkhovsky AB, McQuade KM, Borisy GG. 1997. Analysis of the actin-myosin II system in fish epidermal keratocytes: mechanism of cell body translocation. J Cell Biol 139: 397–415.

Theriot JA, Mitchison TJ. 1991. Actin microfilament dynamics in locomoting cells. Nature 352:126–131.

Vallotton P. 2004. Simultaneous mapping of filamentous actin flow and turnover in migrating cells by quantitative fluorescent speckle microscopy. Proc Natl Acad Sci USA 101:9660–9665.

Vallotton P. 2005. Tracking retrograde flow in keratocytes: news from the front. Mol Biol Cell 16:1223–1231.

Watanabe N. 2002. Single-molecule speckle analysis of actin filament turnover in lamellipodia. Science 295:1083–1086.

Wilson CA, Tsuchida MA, Allen GM, Barnhart EL, Applegate KT, Yam PT, Ji L, Keren K, Danuser G, Theriot JA. 2010. Myosin II contributes to cell-scale actin network treadmilling through network disassembly. Nature 465:373–377.

Wolgemuth CW, Miao L, Vanderlinde O, Roberts T, Oster G. 2005. MSP dynamics drives nematode sperm locomotion. Biophys J 88:2462–2471.

Yam PT, Wilson CA, Ji L, Hebert B, Barnhart EL, Dye NA, Wiseman PW, Danuser G, Theriot JA. 2007. Actin myosin network reorganization breaks symmetry at the cell rear to spontaneously initiate polarized cell motility. J Cell Biol 178:1207–1221.

Zajac M, Dacanay B, Mohler WA, Wolgemuth CW. 2008. Depolymerization-driven flow in nematode spermatozoa relates crawling speed to size and shape. Biophys J 94:3810–3823.

Zimmermann J, Brunner C, Enculescu M, Goegler M, Ehrlicher A, Käs J, Falcke M. 2012. Actin filament elasticity and retrograde flow shape the force-velocity relation of motile cells. Biophys J 102:287–295.